Changes of Subseasonal Variability Associated with El Niño

GILBERT P. COMPO, PRASHANT D. SARDESHMUKH, AND CÉCILE PENLAND

NOAA–CIRES Climate Diagnostics Center, University of Colorado, Boulder, Colorado

(Manuscript received 8 September 2000, in final form 14 February 2001)

ABSTRACT

This paper is concerned with assessing the impact of the El Niño–Southern Oscillation (ENSO) on atmospheric variability on synoptic, intraseasonal, monthly, and seasonal timescales. Global reanalysis data as well as atmospheric general circulation model (AGCM) simulations are used for this purpose. For the observational analysis, 53 yr of NCEP reanalyses are stratified into El Niño, La Niña, and neutral winters [Jan–Feb–Mar (JFM)]. The AGCM analysis is based on three sets of 180 seasonal integrations made with prescribed global sea surface temperatures corresponding to an observed El Niño event (JFM 1987), an observed La Niña event (JFM 1989), and climatological mean JFM conditions. These ensembles are large enough to estimate the ENSO-induced changes of variability even in regions not usually associated with an ENSO effect. The focus is on the anomalous variability of precipitation and 500-mb heights.

The most important result from this analysis is that the patterns of the anomalous extratropical height variability change sharply from the synoptic to the intraseasonal to monthly timescales, but are similar thereafter. In contrast, the patterns of the anomalous tropical rainfall variability are nearly identical across these timescales. On the synoptic and monthly scales, the anomalous extratropical height variability is generally opposite for El Niño and La Niña, and is also roughly symmetric about the equator. On the intraseasonal scale, however, the anomalous height variability is of the same sign for El Niño and La Niña in the Atlantic sector, and is antisymmetric about the equator in the Pacific sector. In the North Pacific, these intraseasonal variance anomalies (which are consistent with a decrease of blocking activity during El Niño and an increase during La Niña) are of opposite sign to the monthly and seasonal variance anomalies.

The sharp differences across timescales in the ENSO-induced changes of extratropical variability suggest that different dynamical mechanisms dominate on different timescales. They also have implications for the predictability of extreme events on those timescales. Finally, there is evidence here that these impacts on extratropical variability may differ substantially from ENSO event to event, especially in the northern Atlantic and over Europe.

1. Introduction

Given that ENSO is arguably the largest predictable signal in the climate system on seasonal to interannual scales, it is not surprising that numerous studies have been devoted to investigating its global impact. Most of these have focused on seasonal mean changes. An ENSO event can, however, also affect the statistics of weather within a season, and perhaps even an individual storm (Barsugli et al. 1999). These effects can be distinct from the effects on seasonal mean quantities, and can have important practical implications. For instance, one may imagine a situation in which El Niño alters the occurrence of both cold waves and hot spells in a winter. The effect is a meaningful change in the risk of extreme weather, even though little seasonal mean signal is evident. Indeed it has been shown (Katz and Brown 1992) that such altered risks of extreme weather are more sensitive to changes of variance than to changes of the mean.

The few published studies of the ENSO effect on subseasonal atmospheric variability, constrained either by sampling requirements or data availability, have formed composites over several ENSO events to diagnose the effect in limited regions (e.g., Fraedrich 1990, 1994; Hoerling and Ting 1994; Renwick and Wallace 1996; Straus and Shukla 1997; Gershunov and Barnett 1998; May and Bengtsson 1998; Renwick 1998; Renshaw et al. 1998; Vincent et al. 1998; Matthews and Kiladis 1999; May 1999; Robertson and Ghil 1999; Renwick and Revell 1999; Smith and Sardeshmukh 2000). In this paper, ENSO-induced changes of subseasonal variability are estimated *globally* from very large ensembles of AGCM integrations for one El Niño [Jan–Feb–Mar (JFM) 1987] and one La Niña (JFM 1989) event. These are then compared with historical changes averaged over 11 El Niño and 11 La Niña events in the recent record. Such a comparison has not been made

Corresponding author address: Dr. Gilbert P. Compo, NOAA–CIRES Climate Diagnostics Center, 325 Broadway, R/CDC1, Boulder CO 80305-3328.
E-mail: compo@colorado.edu

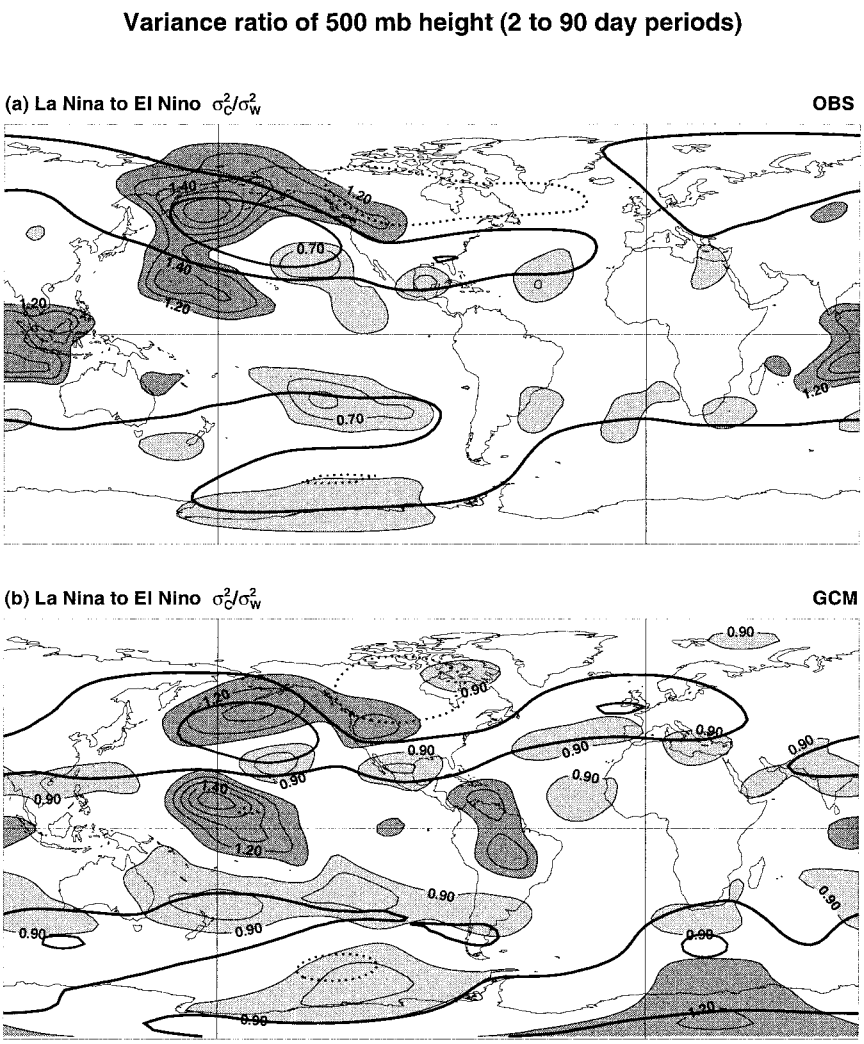

FIG. 1. Shading shows the ratio of 500-mb height subseasonal variance during La Niña winters (JFM) to that during El Niño. The variance is estimated from (a) 11 La Niña and 11 El Niño winters in the NCEP–NCAR 1948–2000 Reanalyses and (b) from the NCEP MRF9 GCM for 60 La Niña (1989) and 60 El Niño (1987) JFM seasonal integrations. Contours in both (a) and (b) are drawn at intervals of 0.1. Increased variance is indicated by dark, and decreased variance by light, shading. The 0.9, 1.0, and 1.1 contours are suppressed in (a), and 1.0 is suppressed in (b). All contours shown are significant near or above the 1% level assuming a two-sided F distribution. The bandpass filter passes all power for periods between 2 and 90 days. Heavy, thick contours show the 500-mb height JFM-mean difference between (a) La Niña and El Niño winters in the NCEP reanalyses and (b) the GCM's La Niña and El Niño JFM ensemble. Contour interval is 40.0 m, and negative values are dotted.

previously, and should be useful in gauging the robustness of the changes of variability, their predictability, and their variation from event to event.

Figure 1 introduces this comparison. The shaded regions show the ratio of wintertime (JFM) subseasonal variance (in the 2–90-day period band) of 500-mb geopotential heights during La Niña to that during El Niño. This ratio emphasizes the linear aspects of the ENSO effect on subseasonal variance. Figure 1a is derived from an observational ENSO composite and Fig. 1b from AGCM ensembles for 1987 and 1989. The observational plot is based on subseasonal variance in 11 El Niño and 11 La Niña winters selected from the National Centers for Environmental Prediction–National Center for Atmospheric Research (NCEP–NCAR) reanalysis dataset (see Table 1). The AGCM plot is derived from the numerical experiment of Sardeshmukh et al. (2000, hereafter SCP) described in section 2. Briefly, three sets of 180 seasonal integrations were made using the NCEP MRF9 AGCM with prescribed observed global sea surface temperatures (SSTs) for the El Niño of JFM 1987, the La Niña of JFM 1989, and

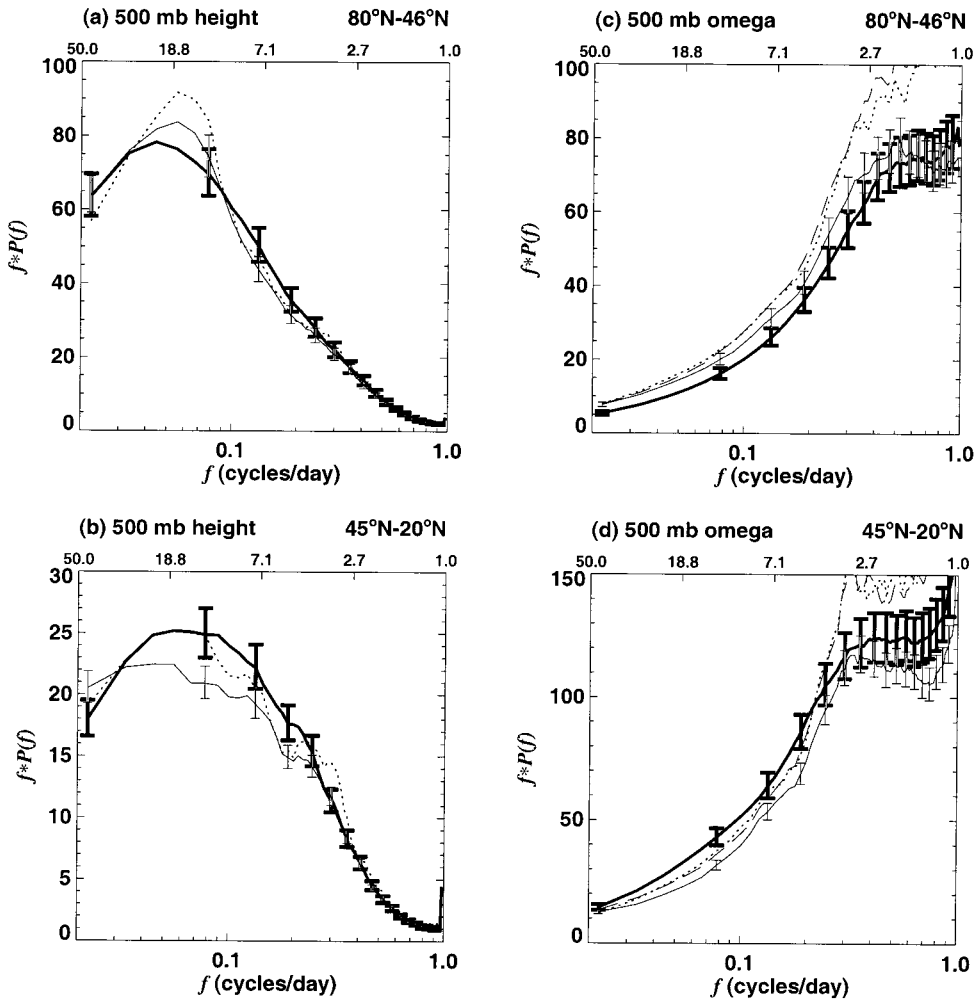

FIG. 2. Comparison of spectra of (a), (b) 500-mb height and (c), (d) 500-mb vertical velocity in (a), (c) high latitudes and (b), (d) midlatitudes. The spectra are estimated from 17 neutral winters (JFM) of NCEP reanalyses (thin curve), 8 neutral winters of chi-corrected NCEP reanalyses [dashed curve, (c), (d)], 5 neutral winters of ECMWF reanalyses (dotted curve), and 90 winter integrations of the MRF9 forced with global seasonally varying climatological SSTs (thick curve). Spectra are zonally averaged, then meridionally averaged (a), (c) from 40° to 80°N and (b), (d) 20° to 45°N. The 95% confidence intervals for the NCEP reanalysis spectra (thin bars) show the expected location of the ''true spectrum,'' while 95% confidence intervals for the GCM (thick bars) show the range expected if only 17 ensemble members were available. Confidence intervals for ECMWF and chi-corrected spectra are suppressed. All spectra have been multiplied by frequency to preserve variance in this semilog representation. Frequency units are cycles day^{-1}. Corresponding periods are indicated. Power spectral density units are (a), (b) mb^2 day^{-1} and (c), (d) mb^2 s^{-2} day^{-1}.

climatological mean JFM conditions. Subsets of these (60 each for El Niño and La Niña, and 90 for climatological SSTs) were used at twice-daily resolution to construct Fig. 1b. The comparison between the observational and GCM panels is not clean: one panel represents a ratio of variances averaged over several events and the other represents the ratio of expected variances for two individual events. Nevertheless, in both Figs. 1a,b changes of order 20%–30% are evident over large regions, with some regions in the North Pacific showing changes of 40%–60%. These changes are substantial even in some regions of zero seasonal-mean signal, indicated by the thick contour. The gross similarity of Figs. 1a,b is reassuring both for the robustness of the changes of variability and this GCM's ability to simulate them. To that extent, the dissimilarity of Figs. 1a,b can be attributed to the comparison not being clean (i.e., event-to-event differences) and, of course, sampling error.

Figure 1 suggests that the linear ENSO-induced changes of total *subseasonal* 500-mb height variability are largely confined to the Pacific sector. This is in contrast to one of SCP's main results that the changes of *seasonal* 500-mb height variability (that is, the different spreads of their seasonal 180-member El Niño and La Niña ensembles) are global in character, and generally

TABLE 1. Northern Hemisphere winters (DJFMA) classified as El Niño, La Niña, and neutral winters in this paper. The year in the table refers to Jan of the event listed. The number below the years is the value of the SST index in the Niño-3.4 area defined in the text.

					El Niño					
1983	1998	1992	1958	1973	1966	1969	1995	1987	1993	1970
1.93	1.90	1.49	1.23	1.04	1.01	0.99	0.93	0.92	0.59	0.54
					La Niña					
1974	1989	2000	1976	1971	1950	1999	1951	1985	1956	1975
−1.57	−1.34	−1.31	−1.30	−1.25	−1.24	−1.11	−0.80	−0.72	−0.71	−0.62
					Neutral					
1980	1990	1982	1948	1953	1957	1979	1952	1961	1954	1997
0.37	0.28	0.20	0.11	0.09	0.05	0.05	0.04	0.03	0.00	−0.02
1960	1981	1986	1963	1984	1972					
−0.05	−0.09	−0.23	−0.26	−0.27	−0.31					

amount to an increase during El Niño and a decrease during La Niña. Figure 1 suggests, if anything, a decrease of subseasonal variance over much of the North Pacific during El Niño relative to La Niña. Extensive diagnosis reported in this paper leads us to conclude that this is not a contradiction: the ENSO effect on 500-mb height variability does indeed depend strongly upon timescale. Specifically, the patterns of the anomalous variability on the synoptic (2–7-day periods), intraseasonal (8–45-day periods) and monthly (30-day average) timescales are all different from one another. On the seasonal (90-day average) scale, however, the anomalous variability is similar to that on the monthly scale.

In this paper, we compare maps of the ENSO-induced anomalous variability during the JFM 1987 El Niño and JFM 1989 La Niña from the above GCM experiment on the synoptic, intraseasonal, and monthly scales, and also compare them, where possible, with corresponding averages over 11 El Niño and 11 La Niña events in the NCEP reanalysis dataset. Our aim is not only to determine how the character of the anomalous variability differs across these subseasonal timescales, but also to get a sense of how it differs for El Niño and La Niña forcing and from ENSO event to event. For brevity, we focus on the anomalous variability of precipitation and 500-mb heights. The former is large in the Tropics and subtropics, and while important in itself, is possibly also important in driving the anomalous extratropical 500-mb height variability. Indeed, SCP argued that the generally larger seasonal 500-mb height variability in their El Niño experiment may have been forced partly by the generally larger seasonal precipitation variability near the equatorial date line.

We present the anomalous variability maps as variance differences rather than ratios, even though statistical significance can be (and here is) established more directly in terms of the latter. Specifically, we present maps of

$$\Delta_\sigma = \frac{\sigma_i^2 - \sigma_o^2}{|\sigma_i^2 - \sigma_o^2|^{1/2}} = \mathrm{sgn}(\sigma_i^2 - \sigma_o^2) \times |\sigma_i^2 - \sigma_o^2|^{1/2}, \quad (1)$$

where i indicates El Niño or La Niña and o indicates climatological (or neutral) SST conditions. This quantity has the same units as the mean ENSO signal, is of comparable magnitude, and preserves the sign of the variance difference. Maps of the ratio σ_i^2/σ_o^2, on the other hand, have very large magnitudes in regions of small σ_o^2 where they also tend to be noisy from sampling errors. Maps of Δ_σ are well behaved, in this regard, and still maintain similar features since the sign of Δ_σ is the same everywhere as that of the variance ratio minus 1, and also of the difference $\sigma_i - \sigma_o$ of the standard deviations. We note in passing that patterns of $\sigma_i^2 - \sigma_o^2$ (and therefore of Δ_σ) are also more directly interpreted and diagnosed than those of σ_i^2/σ_o^2 in terms of the dynamical difference equations for second moment quantities, to be reported in a future publication.

The paper is organized as follows. Section 2 describes the data, SCP's GCM experiment, and the analysis method. In section 3, a comparison is made of reanalysis and GCM-simulated subseasonal variability during winters with neutral tropical SSTs to further assess this GCM's suitability for studying this problem. In section 4 the GCM estimates of ENSO-induced changes of seasonal variability [denoted Δ_σ (seasonal)] are compared with those of monthly variability [Δ_σ (monthly)]. Reanalysis and GCM estimates of ENSO-induced changes of synoptic variability [Δ_σ (synoptic)] and intraseasonal variability [Δ_σ (intraseasonal)] are discussed in sections 5 and 6, respectively. The important issue of ensemble size needed to establish these results is discussed in section 7. Summary global measures of the changes of subseasonal variance are presented in section 8. The consistency or otherwise of our results with previous work on this topic is discussed in section 9. Section 10 follows with some interpretation and implications, and concluding remarks are made in section 11.

2. Data, model experiment, and analysis method

a. Data

For brevity, we focus mainly on precipitation and 500-mb geopotential height in this paper. For a supple-

mental estimate of variability, we also use 500-mb vertical velocity. Analyzed height and vertical velocity fields were obtained from the 53-yr (1948–2000) NCEP–NCAR reanalyses (Kalnay et al. 1996) at twice-daily resolution. Some calculations were also performed with the 1979–93 European Centre for Medium-Range Weather Forecasts (ECMWF) reanalyses (Gibson et al. 1997). Additional estimates of 500-mb vertical velocity were obtained from a ''chi-corrected'' version of the 1964–98 NCEP–NCAR reanalyses (Sardeshmukh et al. 1999). Solution of the so-called baroclinic ''chi problem'' (Sardeshmukh 1993) yields horizontal wind divergence that is consistent with the three-dimensional vorticity and column-integrated mass budgets, leading to revised estimates of vertical velocity. Twice-daily chi-corrected fields were used here. The chi-corrected fields show substantially greater variability than the uncorrected fields at all timescales, and yield vertical profiles of diabatic heating that compare better with observations from the Tropical Ocean Global Atmosphere Coupled Ocean–Atmosphere Response Experiment field experiment than do the NCEP reanalysis data for that period (Sardeshmukh et al. 1999).

The NCEP reanalysis dataset was partitioned into El Niño, La Niña, and neutral years based on an SST index, defined as an average over the Niño-3.4 region (5.0°N–5.0°S, 170°–120°W) using the GISST2.3b SST dataset (Parker et al. 1995). Data for JFM 2000 were taken from the NCEP operational SST analyses (Reynolds and Smith 1994). Niño-3.4 anomalies were constructed by removing a least squares fit to the first three harmonics of the annual cycle and, as suggested by Trenberth (1997), smoothing with a 5-month running mean filter. The SST index was then ranked, and winters (DJFMA) with the highest 11, lowest 11, and middle 17 ranks were classified as El Niño, La Niña, and neutral winters, respectively (see Table 1). The unequal number of categories approximates the unequal number of ensemble members available from the GCM experiment at twice-daily resolution, and has the benefit of increasing the number of samples in the neutral category while excluding weak ENSO events from it. Weak events were also excluded from the active-ENSO categories. The composite SST index values are 1.14°C for El Niño and −1.09°C for La Niña, whose magnitudes are statistically indistinguishable (SCP).

Similar procedures were applied to the 15-yr ECMWF reanalysis and 25-yr chi-corrected datasets. These shorter datasets were also stratified into El Niño, La Niña, and neutral years with five members in each category for the ECMWF reanalyses, and eight members in each category for the chi-corrected data.

b. Model experiment

The NCEP atmospheric GCM used is the MRF9, identical to that used by Kumar et al. (1996), Chen and van den Dool (1997b), and SCP. The model has a spatial discretization of T40 in the horizontal (about 3° lat by 3° long) and 18 sigma (normalized pressure) levels in the vertical. Kanamitsu et al. (1991) describe the NCEP MRF model in detail. The model used here differs from the version of the NCEP model used to assimilate the reanalysis observations in several respects, including horizontal resolution (T40 compared to T62), convective parameterization (Kuo vs Arakawa–Schubert), diagnostic cloud scheme, and soil model. [For the MRF9 and reanalysis models, Kumar et al. (1996) and Kalnay et al. (1996), respectively, provide detailed references of the parameterization schemes used in each model configuration.] The GCM integrations analyzed here are the same as made by SCP. Seasonal integrations were made with observed global climatological JFM SSTs and observed global SSTs for JFM 1987 and JFM 1989. Ensembles of 180 integrations, differing only in initial atmospheric states, were made for each of these three SST boundary conditions. Of these $180 \times 3 = 540$ seasonal integrations, 90 were stored at twice-daily resolution for the climatological JFM SSTs and 60 each for JFM 1987 and JFM 1989.

c. Analysis method

All of our subseasonal results are based upon traditional Fourier analysis of the reanalysis and GCM data. Seasonal and monthly results are based on standard statistics. Anomalies of the reanalysis data were computed by removing a least squares fit to the first three annual harmonics of the 1969–99 NCEP reanalyses and the complete record of the ECMWF and chi-corrected data. For the GCM data, anomalies were derived by removing a least squares fit to the first three annual harmonics of the daily averaged climatological-SST ensemble. The Fourier power spectrum of JFM 90-day anomaly segments was computed for each ensemble member (or each calendar year for the reanalyses) at every grid point. Every spectrum has 45 frequencies that were assumed to have 2 degrees of freedom (dof) each (Jenkins and Watts 1968). The spectra were averaged over all ensemble members with the same SST forcing, or with the same ENSO classification, to form separate spectral estimates at each grid point. At each frequency, this gave $90 \times 2 = 180$ dof for the neutral GCM ensemble, $60 \times 2 = 120$ dof for the El Niño and La Niña ensembles, $17 \times 2 = 34$ dof for the NCEP reanalyses neutral years, and $11 \times 2 = 22$ dof for the NCEP reanalyses El Niño and La Niña classified years. The presented spectra were then smoothed with a 5-frequency boxcar average (Jenkins and Watts 1968). As suggested by Jenkins and Watts (1968), all spectral estimates were assumed to be independent and chi-squared distributed.

Finally, maps of variance changes were constructed on synoptic, intraseasonal, monthly, and seasonal timescales using the definition of Δ_σ in Eq. (1). Two bands are presented: a synoptic band representing storm track activity (e.g., Blackmon et al. 1977) and an intraseasonal

band of the widest possible range representing broadband low-frequency phenomena between synoptic and monthly timescales, such as blocking activity (Dole and Gordon 1983) and low-frequency Rossby waves (Borges and Sardeshmukh 1995). The synoptic bandpass-filtered maps were summed over 33 frequencies from 2.0 to 6.9 days. The intraseasonal bandpass-filtered maps were summed over 11 frequencies from 7.5 to 45 days. Maps for other high-frequency and intermediate frequency bands were also examined and found to give similar results, as discussed in section 8. Field significance was assessed using a bootstrap method (resampling with replacement) and the binomial distribution (Livezey and Chen 1983) and is discussed in detail in the appendix. All maps shown are field significant at or above the 10% level.

3. Climatological variability

In this section, the gross variability of the NCEP MRF9 GCM forced with climatological SSTs is compared with reanalysis estimates of variability during near-neutral ENSO years. Area-averaged spectra are used for this purpose. This approach is similar to that of May (1999), who used a five-member GCM ensemble forced with observed SSTs from 1979 to 1993 and compared its spectra to those obtained from the ECMWF reanalyses for the same period.

Figure 2 presents Northern Hemisphere midlatitude spectra (in a variance-preserving format) of 500-mb height (Figs. 2a,b) and 500-mb vertical velocity (Figs. 2c,d). The spectra are area-averaged over high latitudes (Figs. 2a,c) and midlatitudes (Figs. 2b,d). The estimates are from the GCM ensemble (thick curve), the NCEP reanalyses (thin curve), and the ECMWF reanalyses (dotted curve). Chi-corrected estimates of 500-mb vertical velocity spectra are also shown (dashed curve). The thick vertical bars show the 95% range of variation expected in the location of the GCM spectrum if only 17 members were available as in the NCEP reanalyses. For the NCEP reanalyses spectrum, the thin bars show the 95% confidence interval for the location of the ''true'' spectrum. The confidence intervals for the ECMWF and chi-corrected estimates are suppressed for clarity, but are larger than those for the NCEP reanalyses. It is apparent that the GCM's extratropical variability of both 500-mb heights and vertical velocity is largely within the estimates from the reanalyses for this gross measure. The spectra further suggest that the model underestimates high-latitude variability (particularly in vertical velocity) at periods longer than 10 days.

In contrast to extratropical variability, estimates of tropical variability differ substantially among reanalyses and the GCM (Fig. 3). Figure 3 shows area-averaged spectra of 500-mb vertical velocity between 19°N and 19°S. The estimates are as in Fig. 2c. Tropical vertical velocity is closely (though not exclusively) tied to tropical precipitation in regions of ascent, so its variability

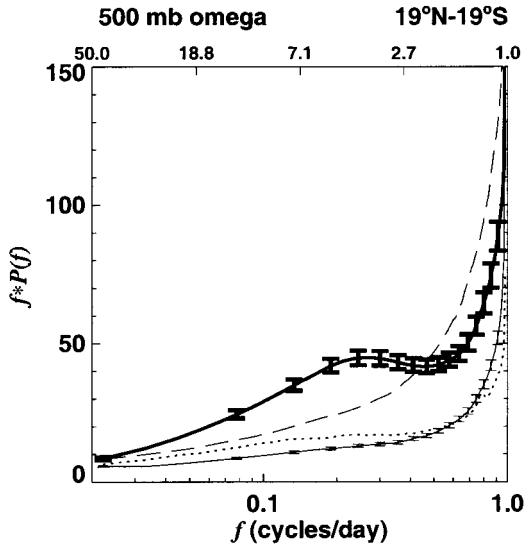

FIG. 3. As in Fig. 2c but for tropical spectra of 500-mb vertical velocity. Confidence intervals are as in Fig. 2. They are suppressed for ECMWF and chi-corrected spectra.

provides some indication of precipitation variability. It is also useful in depicting dynamical variations in regions of diabatic *cooling,* that is, away from regions of strong precipitation. This makes it a broader descriptor of tropical variability than precipitation alone. According to this measure, the ECMWF reanalyses show more tropical variability than the NCEP at periods of 2 days and longer. The comparison suggests that low-frequency tropical variability is underestimated in the NCEP reanalyses, and is significantly enhanced at all frequencies by the chi correction. Nevertheless, substantial observational uncertainties remain in the magnitude of tropical variability at all frequencies. The GCM's synoptic and intraseasonal tropical variability are apparently outliers compared to the various observational estimates. However, the magnitudes of low-frequency variability appear to be reasonable, and the very high-frequency (1.0–2.5 days) variability lies between the chi-corrected and NCEP and ECMWF estimates.

The above result is consistent with the recent study of Newman et al. (2000), who compared tropical outgoing longwave radiation and tropical divergence estimates from the ECMWF, National Aeronautics and Space Administration, and NCEP reanalyses and concluded that none could reliably represent the structure or magnitude of upper-tropospheric divergence variability at seasonal or intraseasonal timescales. Despite the observational uncertainties, however, the results below should be viewed bearing in mind that the MRF9 GCM may well overestimate tropical variability on synoptic and intraseasonal timescales.

4. Changes of seasonal and monthly variance

SCP found coherent large-scale changes in the variability of JFM averages (i.e., in the spread of their 180-

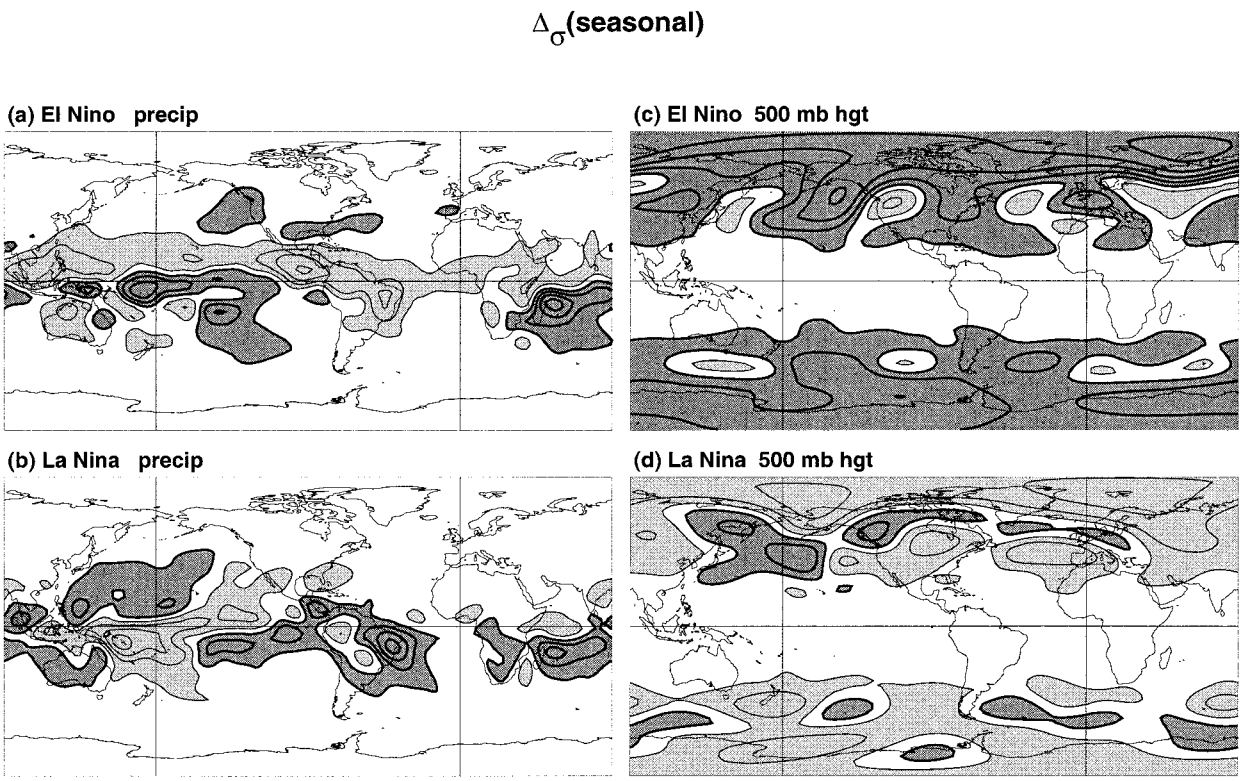

FIG. 4. JFM Δ_σ (seasonal) for (a), (b) precipitation and (c), (d) 500-mb height between the (a), (c) El Niño and neutral GCM ensembles and (b), (d) La Niña and neutral GCM ensembles. Each ensemble contains 180 members. Contours in the precipitation plots are drawn at intervals of 1.0 mm day^{-1} starting at 0.5 mm day^{-1}. Those in the 500-mb height plots are drawn at intervals of 16.0 m starting at 8.0 m. All seasonal variances have been multiplied by 3 before differencing. Dark (light) shading indicates positive (negative) values. Adapted from Sardeshmukh et al. (2000).

member seasonal ensembles) for both warm and cold tropical SST forcing. Figure 4 is adapted from that result and shows Δ_σ (seasonal) of precipitation (Figs. 4a,b) and 500-mb height (Figs. 4c,d) for El Niño (Figs. 4a,c) and La Niña (Figs. 4b,d). All seasonal variances have been multiplied by a factor of 3 for a more direct comparison with the changes of monthly variability to follow. This accounts for the fact that the variance of 3-month seasonal averages is approximately one-third the variance of monthly averages (Schubert et al. 2001). The local and field significance of these panels was discussed previously by SCP. The important features to note are 1) to a first approximation, the changes of spread of both precipitation and 500-mb height are of opposite signs for El Niño and La Niña, as seen, for instance, in the western Pacific and South American regions for precipitation and in high latitudes for 500-mb height; 2) the changes of precipitation spread are largely confined to the Tropics; and 3) the changes of 500-mb height spread are largely confined to the extratropics. Note that Fig. 4 suggests generally *greater* variability of seasonal 500-mb heights during El Niño than La Niña.

The patterns of Δ_σ (monthly) in Fig. 5 are similar to those in Fig. 4. Figure 5 shows the February Δ_σ (monthly) in the same format as Fig. 4, but without the factor-of-3 scaling of the variance. It is evident that the ENSO-induced changes of monthly precipitation and 500-mb height variability have nearly the same structure as those of seasonal variability. Some small regions, such as the southeastern United States during La Niña, however, do show a marked difference.

Figures 5a,b suggest that in some regions at least, El Niño and La Niña may alter monthly precipitation variance in the same direction. This is particularly striking over the southwest Indian Ocean, east of Australia, the eastern equatorial Pacific, and the southeastern United States. These were also identified as areas of interesting ''nonlinear'' responses to ENSO by SCP.

Note that these results were obtained using the full-sized 180-member ensembles for El Niño, La Niña, and neutral SST conditions. A discussion of a minimum ensemble size needed to reproduce the seasonal changes (which as noted above are roughly a factor of 3 weaker than the monthly changes) is deferred until section 7.

5. Changes of synoptic variance

Figure 6 shows Δ_σ (synoptic) of Northern Hemisphere 500-mb heights during El Niño (Figs. 6a,c) and La Niña

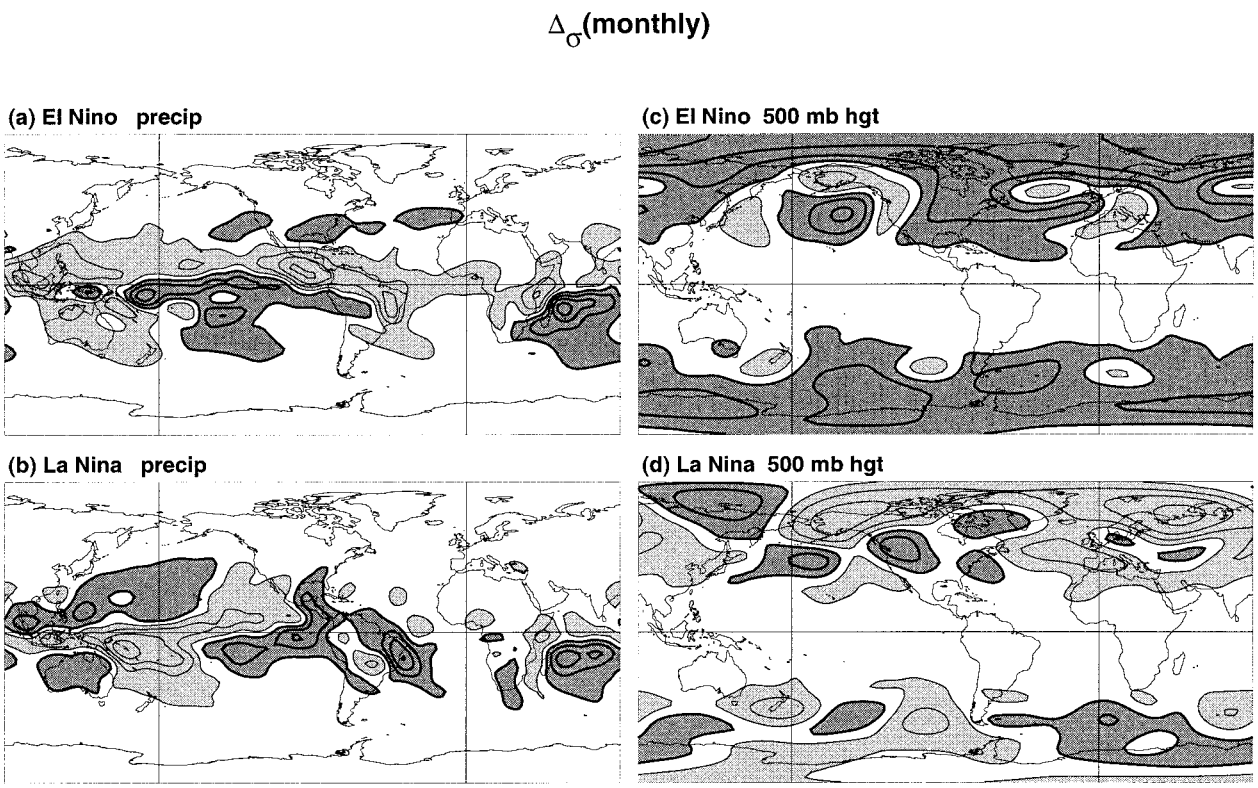

FIG. 5. Same as Fig. 4 but for Feb Δ_σ (monthly). All ensembles have 180 members each. Note that no scaling has been applied to these variances.

(Figs. 6b,d) estimated from the NCEP reanalyses (Figs. 6a,b) and our GCM experiment (Figs. 6c,d) Thick contours indicate increased variance, and thin contours indicate decreased variance. Shading highlights regions locally significant above the 10% level using a two-sided F test.

As already noted for other scales, the comparison of the reanalysis and GCM-simulated Δ_σ (synoptic) is also not clean. Still, several of the gross features identified in previous studies are reproduced, particularly in the El Niño simulation, such as shifted storm tracks over the Pacific Ocean and North America (e.g., Lau 1988; Hoerling and Ting 1994; Straus and Shukla 1997; May and Bengtsson 1998). The enhanced variability over east Asia during El Niño was noted previously by Straus and Shukla (1997) in their single-member GCM simulation of three El Niño events. Straus and Shukla (1997) concluded, however, that this was probably due to GCM error. Note that in Fig. 6, the east Asian positive Δ_σ (synoptic) occurs in both the reanalysis and GCM panels. The agreement lends credence to the reality of such ENSO-induced changes, and this GCM's ability to represent them.

Several new features are evident in the reanalysis and GCM panels of Fig. 6 that are significant both because of the large number of samples and their mutual consistency. For example during El Niño, a belt of positive Δ_σ (synoptic) extends from the Mediterranean and northeastern Africa, across Asia and the Pacific, into the eastern Atlantic. A region of decreased variance is seen to the north. This coherent hemispheric response has not been noted previously in the literature. It represents an El Niño impact on daily weather, sometimes even in regions of near-zero seasonal-mean differences of 500-mb height, such as over south Asia in Fig. 1.

In the North Atlantic and European sector, the reanalysis composites differ from the GCM results for the individual events of 1987 and 1989. This suggests that the expected changes of synoptic variability in this region may differ from ENSO event to event.

Figure 7 shows Δ_σ (synoptic) of precipitation (Figs. 7a,b) and 500-mb height (Figs. 7c,d) in the same format as Fig. 4, but with different contour intervals. The pattern for precipitation is essentially the same as in Figs. 4 and 5. The asymmetries between the El Niño and La Niña changes noted there are again evident here over the east equatorial Pacific, southwest Indian Ocean, and especially, to the north of New Zealand. The pattern for 500-mb heights in Fig. 7, on the other hand, is strikingly different from that of Figs. 4 and 5. It shows alternating regions of decreases and increases in both hemispheres that are roughly symmetric about the equator. This symmetry is especially clear in the Pacific along the date line in the La Niña case, but is also evident in several other longitude sectors. Note that Figs. 7a,b show no such symmetry about the equator. The synoptic height

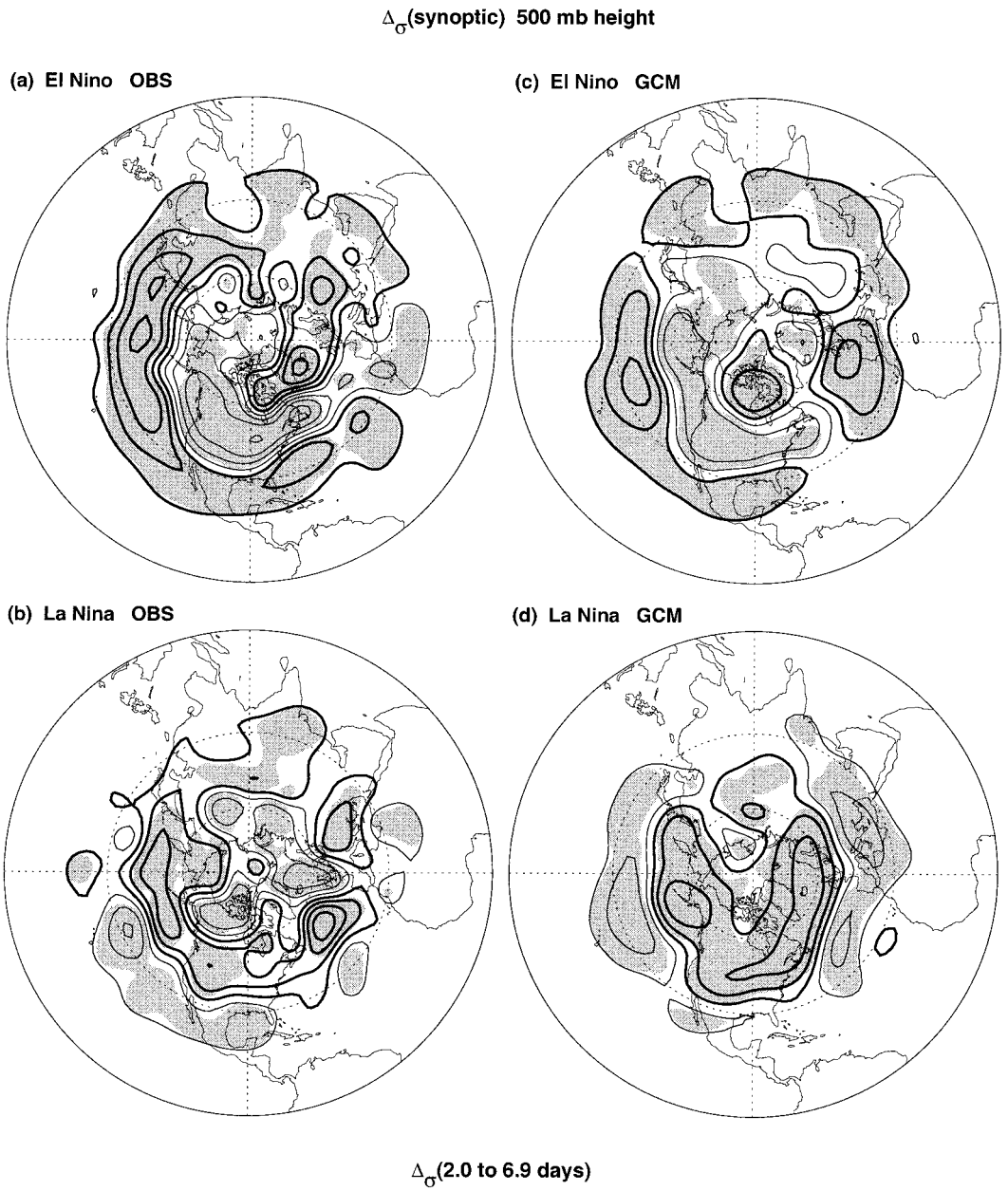

FIG. 6. The Δ_σ (synoptic) for 500-mb heights between (a), (b) ENSO and neutral winters in the NCEP reanalyses and (c), (d) the GCM ensembles. Results are shown for (a), (c) El Niño minus neutral and (b), (d) La Niña minus neutral. Line contours in all panels are drawn at 8.0-m intervals starting at 4.0 m. Thick (thin) contours indicate positive (negative) values. Shading shows those regions locally significant at or above the 10% level using a two-sided F test.

variability changes are generally opposite for El Niño and La Niña, but with a slight tendency for more zonal symmetry during La Niña, especially in high latitudes.

6. Changes of intraseasonal variance

The ENSO impact on 500-mb height synoptic variability in Fig. 7 (2–7-day scales) is substantially different from the ''linear'' effect on total subseasonal variability in Fig. 1b (2–90-day scales). This is especially true over northern Europe. This suggests that changes of intraseasonal variability (8–45-day scales) may be different from the synoptic, which we confirm below.

Figure 8 shows the similarities and important differences between the Δ_σ (intraseasonal) for 500-mb height estimated from NCEP reanalyses and the GCM. It is in the same format as Fig. 6, but with a different contour interval. As in Fig. 6, comparing the reanalysis composite and the GCM is not clean. The similarity, then, between the El Niño estimates over the Asian, Pacific,

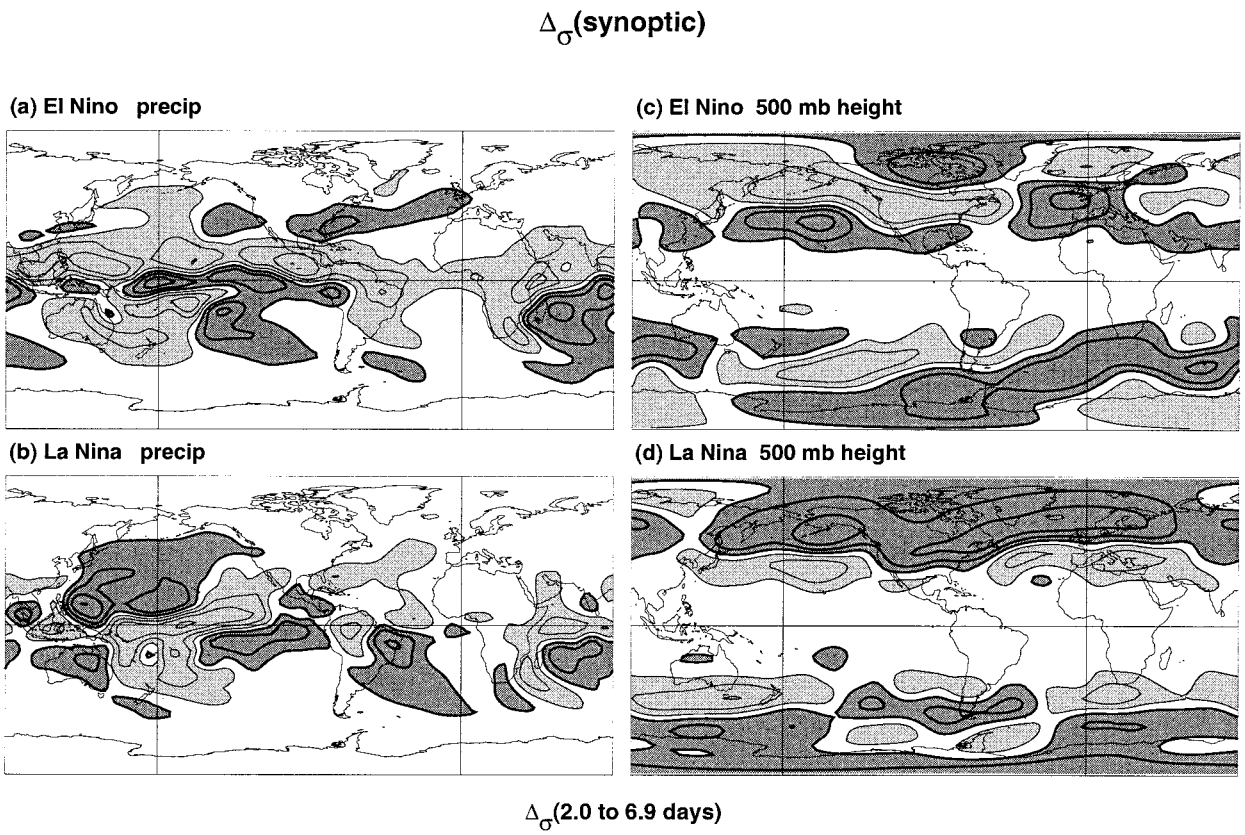

FIG. 7. As in Fig. 4 but for (a), (b) Δ_σ (synoptic) precipitation and (c), (d) 500-mb height between (a), (c) the El Niño and neutral GCM ensembles and (b), (d) La Niña and neutral GCM ensembles. Contours in the precipitation plots are drawn at intervals of 2.0 mm day^{-1} starting at 1.0 mm day^{-1}. Those in the 500-mb height plots are drawn at intervals of 8.0 m starting at 4.0 m. Dark (light) shading indicates positive (negative) values.

and North American regions is encouraging, suggesting that the GCM does have some sensitivity on this timescale to ENSO SST conditions. The negative Δ_σ (intraseasonal) in the North Pacific during El Niño and positive during La Niña is consistent with several studies suggesting that ENSO alters blocking activity in the region (Renwick and Wallace 1996; Chen and van den Dool 1997a, 1999). In Fig. 8d, over the North Pacific, the increased variance is farther east than in the reanalysis data. Whether this shift reflects a model bias or a detail associated with the 1989 SSTs will need to be examined in other cases. Over the north Atlantic and European sectors, the reanalysis and GCM fields compare poorly. Given the relatively good comparison over the rest of the hemisphere, particularly for El Niño, the striking discrepancy seen in the North Atlantic and European region for both the synoptic and intraseasonal timescales raises the possibility that the variability in this region is sensitive to interevent differences in tropical SST forcing.

Figure 9 shows the Δ_σ (intraseasonal) for precipitation and 500-mb height in an identical format to Fig. 4. The pattern for precipitation is again similar to that on the synoptic, monthly, and seasonal scales. The pattern for 500-mb heights is again different. It is substantially antisymmetric about the equator in the Pacific sector, and substantially symmetric in the Atlantic sector, especially during La Niña. Note that while the values of 500-mb height Δ_σ (intraseasonal) are generally of similar magnitude and opposite sign for El Niño and La Niña, they are negative for both ENSO phases in the Atlantic and European sectors. This decrease of intraseasonal variance could be reflected in a decrease of blocking activity, especially over Scandinavia and Iceland, and needs to be investigated using long observational records in which the impact of El Niño and La Niña can be examined separately with statistical confidence.

A comparison of Δ_σ (intraseasonal) in Fig. 9 with Δ_σ (seasonal) and Δ_σ (monthly) in Figs. 4 and 5 is revealing in another respect. For 500-mb heights, the changes in the Northern Hemisphere high latitudes are nearly opposite between the timescales, with El Niño showing a decrease of intraseasonal variability but an increase of monthly and seasonal variability. Over much of the Southern Hemisphere, however, Δ_σ (seasonal), Δ_σ (monthly), and Δ_σ (intraseasonal) have the same sign, with increased variance during El Niño and decreased variance during La Niña. We stress again that the pat-

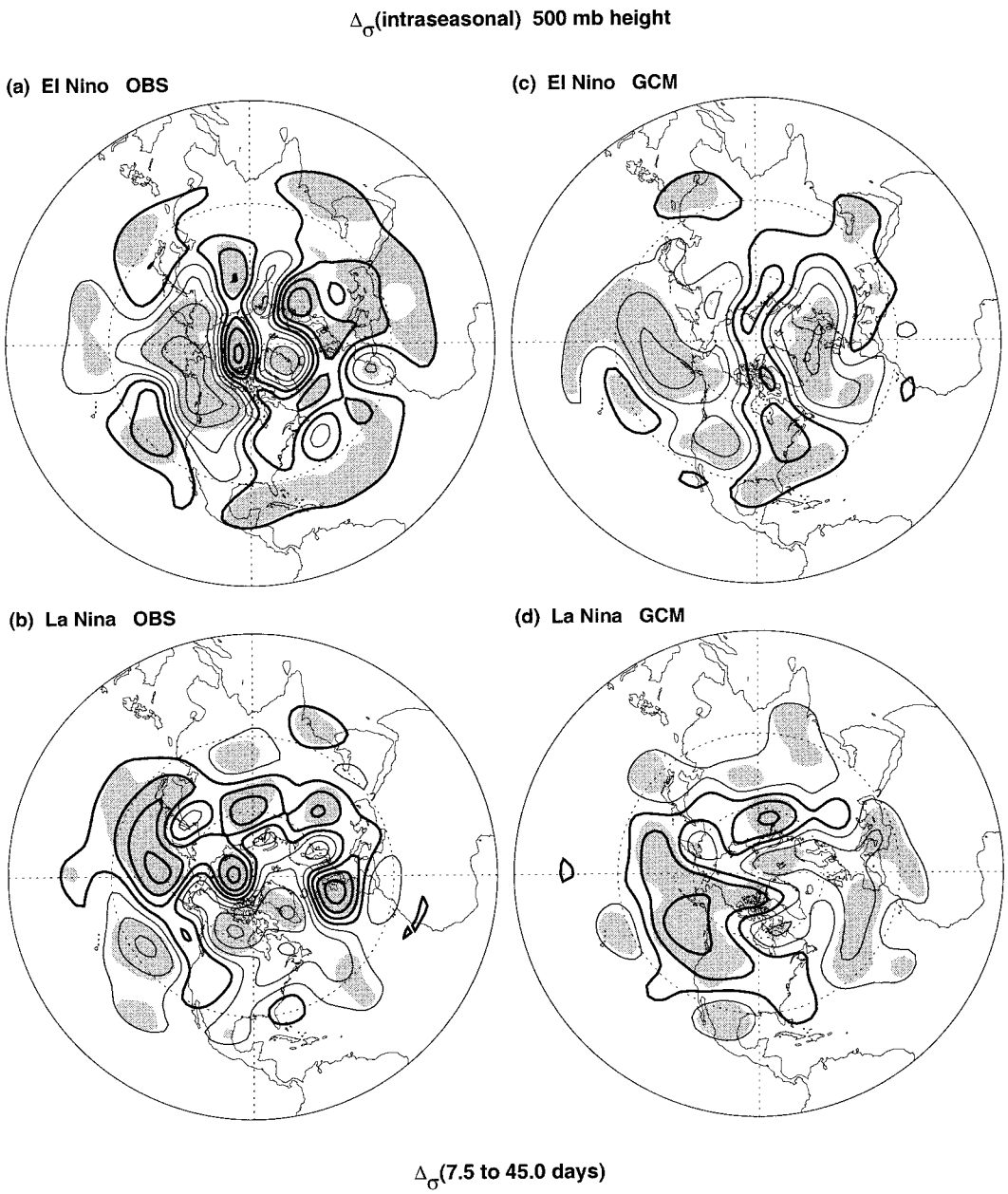

FIG. 8. Same as Fig. 6 but for Δ_σ (intraseasonal) of 500-mb heights. Line contours in all panels are drawn at 16.0-m intervals starting at 8.0 m.

terns for changes of precipitation variability are essentially identical across these timescales.

The sharp change in the character of Δ_σ from intraseasonal to monthly timescales for Northern Hemisphere 500-mb heights may suprise some readers. One might wonder if this is partly due to our having used 180 members for calculating Δ_σ (monthly) but only 60 for calculating Δ_σ (intraseasonal). To eliminate this possibility, we recomputed 500-mb Δ_σ (monthly) using the same 60 members for JFM 1987 and the same 60 members for JFM 1989 that were available for the Δ_σ (intraseasonal) calculations. The resulting maps (not shown) were very similar to those using all 180 members in Fig. 5 with pattern correlations of 0.86 and 0.80 for El Niño and La Niña, respectively.

7. Consideration of ensemble size

Barnett et al. (1994) suggested that an ensemble size of at least 20 members is needed to predict ENSO effects accurately in the midlatitudes. SCP presented a multivariate expression for the effect of ensemble size *n* on

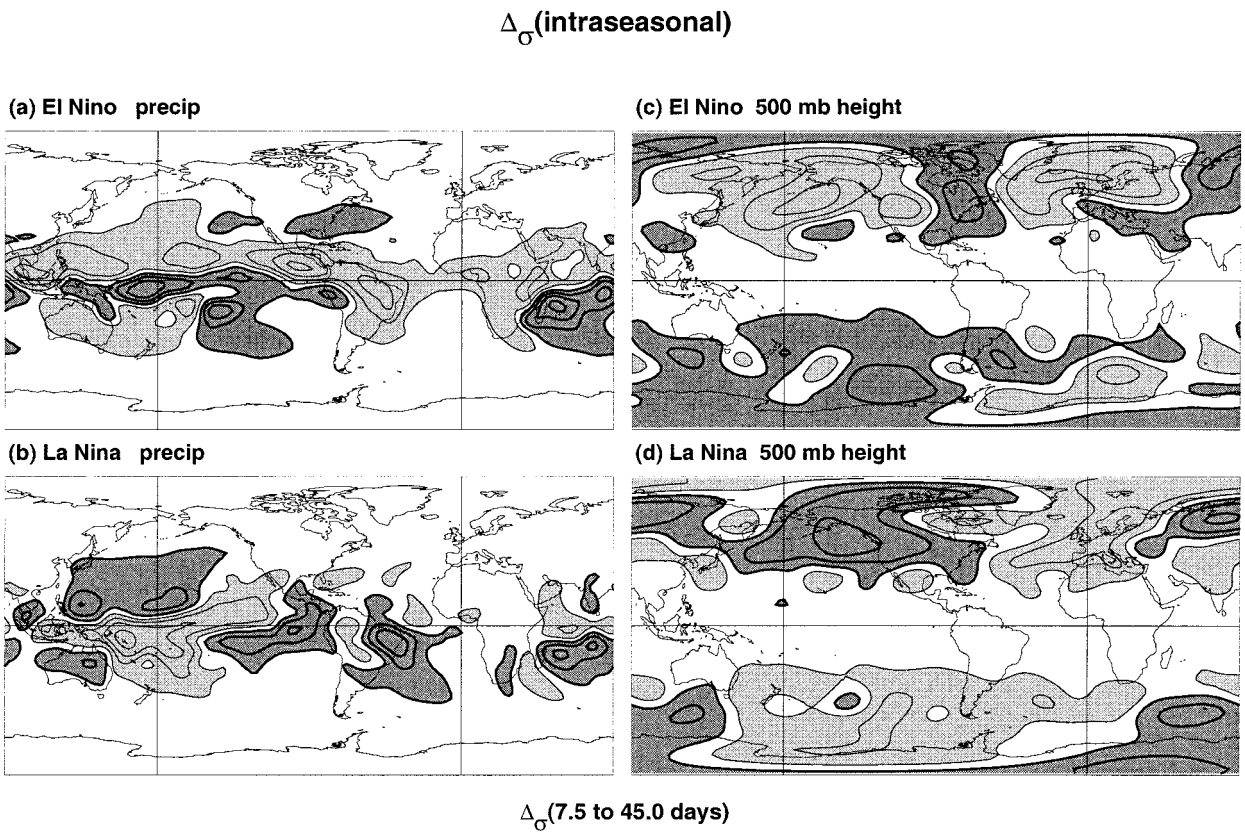

FIG. 9. Same as Fig. 7 but for (a), (b) Δ_σ (intraseasonal) precipitation and (c), (d) 500-mb height. Contours in the precipitation plots are drawn at intervals of 2.0 mm day^{-1} starting at 1.0 mm day^{-1}. Those in the 500-mb height plots are drawn at intervals of 16.0 m starting at 8.0 m. Dark (light) shading indicates positive (negative) values.

the expected correlation skill ρ of an ensemble-mean anomaly forecast as a function of the magnitude of the anomaly state vector x and the covariance matrix of the ensemble C_0. They suggested that most of the realizable gain in forecast skill could be attained with 25 members. However, SCP also pointed out that accurately ascertaining the signal-to-noise ratio, which determines the predictability of the signal and the reliability of an ensemble-mean forecast, requires much larger ensembles. The changes of spread found by them and shown in Fig. 4 impact significantly upon the signal-to-noise ratio of ENSO-induced seasonal mean anomalies. As such, accurate diagnosis of the altered spread is needed. In this connection, it is important to recognize that the spread (or variance) estimated with a small ensemble may not accurately reflect that obtained with a much larger ensemble.

Figure 10 highlights the need for large ensemble sizes to determine the relatively small but meaningful ENSO-induced changes in the variance of seasonal means. Figures 10a,b show 500-mb height Δ_σ (seasonal) for El Niño and La Niña, as in Figs. 4c and 4d, but using only the first 30 of our 180 ensemble members for each SST forcing. The shading indicates regions that are locally significant at the 10% level, with magnitudes greater than 8.0 m. Figures 10a,b are approximately consistent with the ensemble size used by Schubert et al. (2001) in their experiments with the Goddard Earth Observing System-2 AGCM. Schubert et al. (2001) found that the 1983 El Niño had less seasonal variance than the 1989 La Niña over the North Pacific and western North America. Comparing their Fig. 1 with our Fig. 10, the changes of variance between the 1987 El Niño and 1989 La Niña using 30 members are not inconsistent with their result. Areas in the North Pacific in Fig. 10 are locally significant when comparing El Niño to La Niña (not shown), but not when comparing to neutral conditions. Using only 30 members, neither the El Niño nor the La Niña variance difference from neutral is field significant at even the 20% level based on Monte Carlo resampled distributions.

Figures 10c,d show Δ_σ (seasonal) as in Figs. 10a,b, but now using the first 100 ensemble members. The Southern Hemisphere signal is now well resolved (compared to Fig. 4) with 100 members. Most of the El Niño increase in the Northern Hemisphere is also resolved. Indeed, the error of sign over the North Pacific and the South Atlantic is now corrected. With 150 members (not

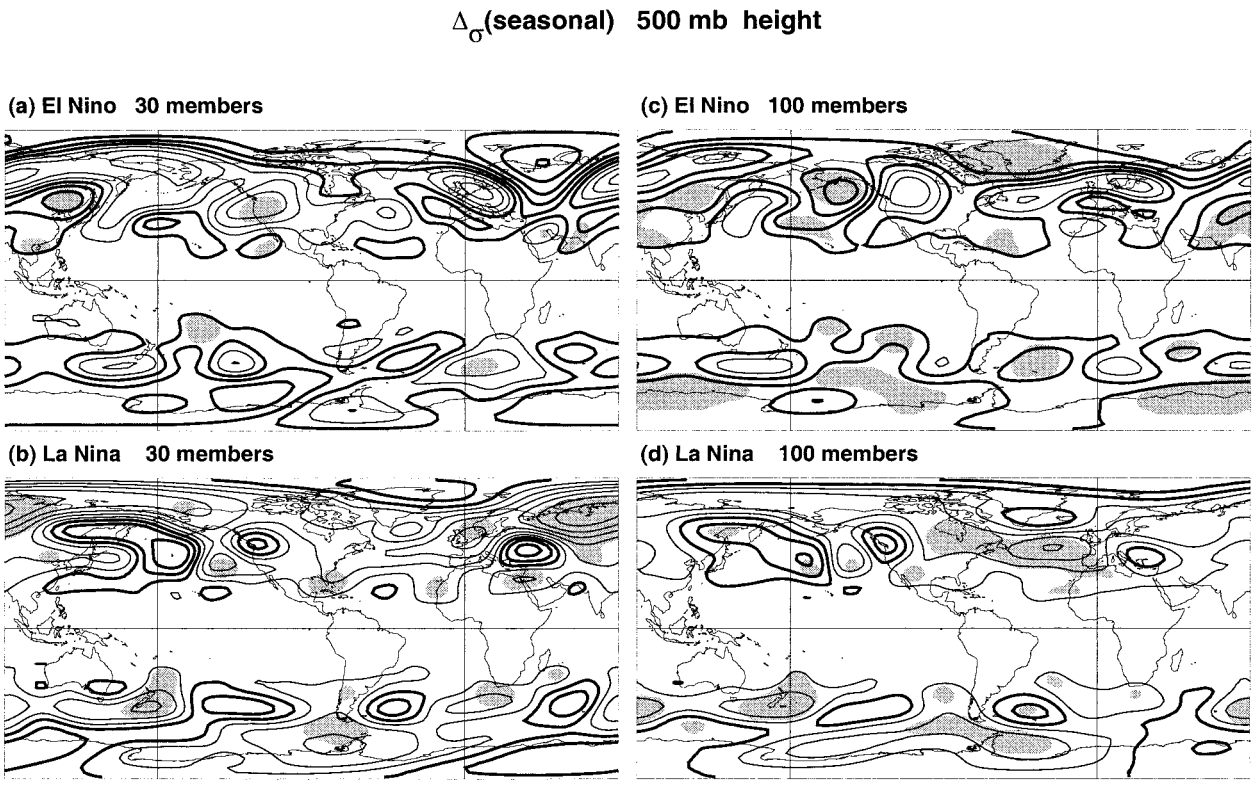

FIG. 10. The Δ_σ (seasonal) for JFM-mean 500-mb height between subsamples of (a), (c) the El Niño and neutral GCM ensembles and (b), (d) La Niña and neutral GCM ensembles using only (a), (b) 30 members in each ensemble and using only (c), (d) 100 members in each ensemble. Line contours are drawn at intervals of 16.0 m starting at 8.0 m. Thick (thin) contours indicate positive (negative) values. Shading shows those values locally significant at the 10% level using a two-sided F test. All seasonal variances have been multiplied by 3 before differencing.

shown), the La Niña Northern Hemisphere Δ_σ (seasonal) is essentially identical to that in Fig. 4. It is important to recognize, however, that convergence to the ''truth'' in Fig. 4 does not occur *uniformly* as ensemble size is increased. We find that with the first 120 members, the areal coverage of locally significant Δ_σ (seasonal) actually *decreases* for La Niña before increasing again (not shown).

How many ensemble members are actually needed? From elementary considerations of commonly used statistical distributions, we suggest below that 150 may be necessary for the seasonal prediction problem. As noted by Wehner (2000) in the context of seasonal means, the answer depends on subjectively specifying a desired level of accuracy, and for his choices ranges from 10 to 200 depending on geographical location. SCP provided useful ''rules of thumb'' for the ensemble size needed to demonstrate both significant mean anomalies and variance changes. In the case of variance and variance changes, the applicable distributions for calculating confidence intervals are the chi-squared (χ^2) and Fisher's F distribution, respectively. Unlike means, the confidence intervals for variance and variance changes depend on the value computed and are asymmetric with respect to that value. For illustrative purposes, let us consider 90% confidence intervals and equal numbers of samples in our control and experimental distributions. Then, given a variance estimate $\hat{S}^2$, the true value σ^2 lies (with 90% confidence) within the interval:

$$\sigma^2 = \left[\frac{\nu\hat{S}^2}{\chi^2_\nu(0.95)}, \frac{\nu\hat{S}^2}{\chi^2_\nu(0.05)}\right], \tag{2}$$

where $\chi^2_\nu(p)$ is the chi-squared distribution with ν degrees of freedom evaluated at probability p. Similarly, given a variance ratio estimate $r = \hat{S}_1^2/\hat{S}_2^2$, the true ratio σ_1^2/σ_2^2 lies within the interval:

$$\frac{\sigma_1^2}{\sigma_2^2} = \left[\frac{r}{F_\nu(0.95)}, \frac{r}{F_\nu(0.05)}\right], \tag{3}$$

where $F_\nu(p)$ is the F distribution with equal degrees of freedom, ν.

Now, for a 30 member ensemble, $\nu = 29$, $29/\chi^2_{29}(0.05) = 0.68$, and $29/\chi^2_{29}(0.95) = 1.64$. The true variance thus lies within about 30%–60% of the calculated variance. The range of the ratio of variances goes from $1/F_{29}(0.95) = 0.537$ to $1/F_{29}(0.05) = 1.86$. The true ratio could

thus be different from that calculated by 50%–80%. These confidence intervals are too wide to allow reliable detection of the 40% (and weaker) ENSO-induced changes of seasonal extratropical variance found by SCP. In general, they are also too wide to give useful estimates of ensemble spread for judging the reliability of an ensemble mean forecast (SCP).

Unfortunately, narrowing these confidence intervals requires much larger ensembles. A 22%–27% range on the variance and a 30% range on the variance ratio does not occur for ensembles of less than 150 members. Note that this represents a 10% accuracy on the standard deviation. To illustrate further, a 10% accuracy on the variance and 15% accuracy on the variance ratio are not reached until 500 ensemble members are used. In view of current computational constraints, an ensemble size of 150 represents a reasonable compromise of what is needed to determine the modest but important ENSO-induced changes of seasonal and monthly variance.

8. Signature of variance changes in global spectra

It is clear from the foregoing that the ENSO-induced changes of extratropical 500-mb height variability depend on timescale. This raises a question of whether these results are sensitive to our precise choice of discrete frequency bands.

To test this, maps of Δ_σ have also been constructed for other frequency bands (not shown). The 500-mb height Δ_σ patterns for other synoptic bands (2.5–6.0, 1.0–7.5 days) are similar to those in Figs. 6 and 7 with extratropical pattern correlations between 0.88 and 0.97. The patterns for other intraseasonal bands (6.0–30.0, 10.0–30.0, and 8.18–90.0 days) are also similar to those in Figs. 8 and 9, with extratropical pattern correlations between 0.76 and 0.90. The reanalysis La Niña composites show the greatest sensitivity to the choice of intraseasonal band, with pattern correlations falling as low as 0.76. The correlations for all other configurations exceed 0.83.

Figure 11 depicts the ENSO impact on the extratropical subseasonal variability of 500-mb heights as a continuous function of frequency. Spectra of 500-mb height from the El Niño ensemble are area averaged and compared as a ratio to similarly averaged spectra from the neutral ensemble (thick curve). This is done for high latitudes (Figs. 11a,c) and middle latitudes (Figs. 11b,d) and also for the Northern Hemisphere (Figs. 11a,b) and Southern Hemisphere (Figs. 11c,d). The thin curve shows the ratio of similarly averaged spectra from the La Niña and neutral ensembles. Horizontal dashed lines indicate the 10% significance level based on a two-sided F test.

These normalized spectra suggest that the ENSO-induced variance changes shown in the previous sections over selected frequency bands are robust across a continuous range of frequencies. The frequency dependence of the ENSO impact is most evident in northern high latitudes where, even in this smooth measure, the response at high frequencies is opposite to that at low frequencies. Although most prominent in the Southern Hemisphere midlatitudes, the increase of low-frequency variance during El Niño is also discernible in other regions, as is the decrease during La Niña. El Niño also induces an increase of high-frequency variance in the midlatitudes of both hemispheres (Figs. 11b,d), and La Niña induces a decrease.

9. Comparison with previous work

Previous work describing an ENSO effect on synoptic variability has found the dominant signal to be a southward shift of the Pacific storm track during El Niño and a northward shift during La Niña, associated with shifts of the Pacific jet (e.g., Lau 1988; Hoerling and Ting 1994; Straus and Shukla 1997; May and Bengtsson 1998; Matthews and Kiladis 1999). This is entirely consistent with the results of Fig. 6. May and Bengtsson (1998) used a five-member ensemble of the ECHAM3 AGCM integrated from 1979 to 1992 to construct El Niño and La Niña composites, based on three events each, of high-frequency 300-mb kinetic energy in the Northern Hemisphere. Their Fig. 11 is consistent with our GCM results for the 1987 El Niño and 1989 La Niña in Fig. 6. In particular, the sign and pattern of the variance changes are nearly the same over the Atlantic sector (although their El Niño change was not locally significant). Given this agreement, the differences between the reanalysis and GCM panels of Fig. 6 may reflect event dependence and not necessarily GCM error.

The extratropical Δ_σ (intraseasonal) values over the Pacific in Figs. 8 and 9 are also largely consistent with previous observational studies. A number of studies have suggested that, in the North Pacific, El Niño decreases blocking activity while La Niña increases it (Renwick and Wallace 1996; Chen and van den Dool 1997a, 1999). Chen and van den Dool (1997a) found in reanalysis data and a GCM experiment that deep trough activity is similarly altered in the North Pacific. These results are consistent with the overall change of intraseasonal variance seen in Fig. 8. The asymmetry of Δ_σ (intraseasonal) about the equator in the Pacific sector for El Niño (Fig. 9c) is similar to that observed by Renwick (1998) and Renwick and Revell (1999). These authors found that blocking activity increases in the South Pacific during El Niño compared to all other years. This is opposite to what occurs in the North Pacific.

The relatively large number of ENSO events in our reanalysis composite, and very large number of ensemble members in our GCM experiment, lend weight to these previous results on the ENSO effect on intraseasonal variability and bolster confidence in their robustness. Still, the GCM's predicted decrease of intraseasonal variance in Fig. 8 over the Atlantic conflicts with the reanalysis composite. It is possible that Δ_σ (intra-

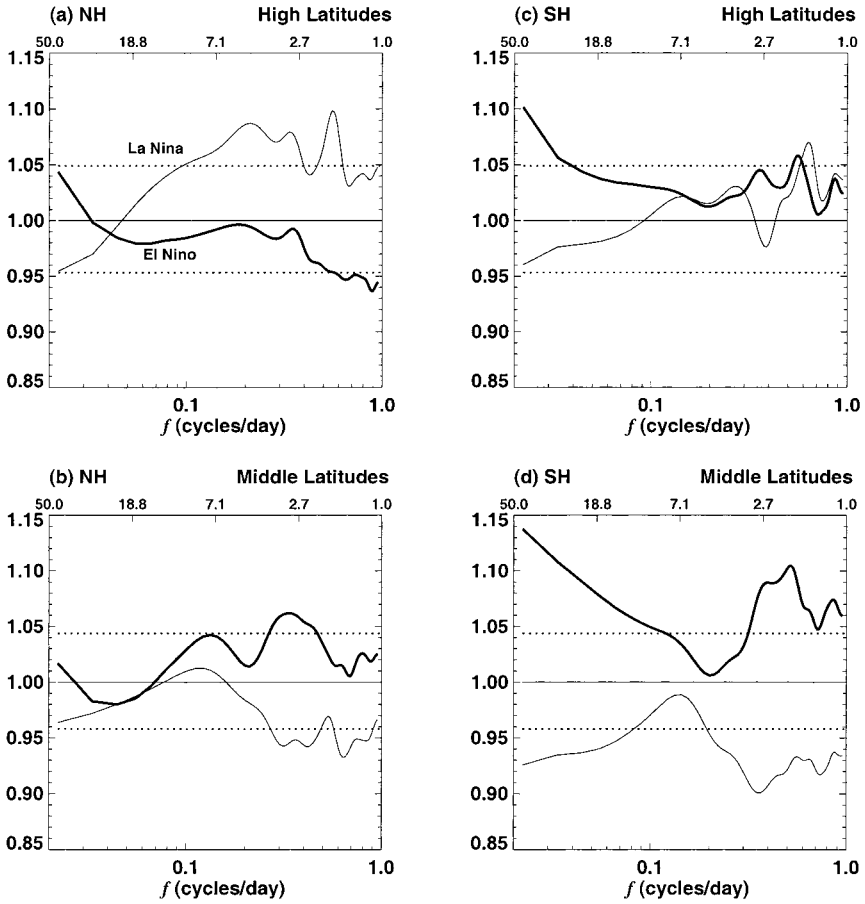

FIG. 11. Thin (thick) curve shows the ratio of 500-mb height spectra during La Niña (El Niño) winters to that during neutral winters. Spectra are zonally averaged, then meridionally averaged from (a), (c) 46° to 80° and (b), (d) 20° to 45° lat in (a), (b) the Northern Hemisphere and (c), (d) the Southern Hemisphere. All spectra are estimated from the GCM experiment. Frequency units are cycles day^{-1}. The dashed lines show the 10% significance level assuming a two-sided F test.

seasonal) in this region is ''nonlinear'' and/or depends on the details of individual ENSO SST forcing patterns. SCP had also highlighted a highly asymmetric seasonal mean response to ENSO phase over the North Atlantic.

In this set of integrations, we do not find the response of May (1999) that El Niño and La Niña both decrease intraseasonal variability in the northern high latitudes (Fig. 11a). Nor is such a change evident in composite spectra derived from NCEP reanalysis data (not shown).

The consistency of our tropical precipitation Δ_σ from synoptic to seasonal timescales in the Indian and Pacific Oceans can also be discerned in the results of Vincent et al. (1998). In that study (their Fig. 7), outgoing longwave radiation variance anomalies were composited in 6–25- and 25–70-day bands based on five El Niño events. An overall similarity to our El Niño results is evident, including an increase of variance in both bands in the southern Indian Ocean. Their observational result further supports our new finding that, overall, ENSO alters variance in the Tropics similarly across timescales.

10. Interpretation and implications

The general agreement of the GCM and reanalysis results in Figs. 1, 6, and 8 and the comparison with previous work suggest that the changes of variability identified here are real and warrant further consideration. We first discuss some apparent disagreements between the ENSO effect shown in Figs. 1 with that in Figs. 6 and 8. We then suggest dynamical interpretation of the ENSO-induced variability changes, hypothesize physical mechanisms, and describe the implications for the seasonal prediction problem.

A comparison of the ''linear'' ENSO impact on the total subseasonal (2–90 days) variability of 500-mb heights in Fig. 1 with Δ_σ (synoptic; in Figs. 6 and 7) and Δ_σ (intraseasonal; in Figs. 8 and 9) suggests an apparent contradiction. In Fig. 1, the statistically significant changes are confined largely to the Pacific sector and no significant changes are seen in several other areas (particularly in the Atlantic sector poleward of 45°)

where both Δ_σ (synoptic) and Δ_σ (intraseasonal) show an ENSO impact. The apparent contradiction arises from the fact that in several of the insignificant areas in Fig. 1, the Δ_σ (synoptic) and Δ_σ (intraseasonal) values are of opposite sign for El Niño as well as La Niña. This makes the total Δ_σ (subseasonal) small. In some regions, Δ_σ is also of the same sign for El Niño and La Niña, and thus has a relatively minor impact on the variance ratio. Both of these effects result in a weak *linear* ENSO impact on the *total* subseasonal variance ratio in Fig. 1.

Figure 1 was intended primarily as a gross measure of the historical ENSO impacts on subseasonal variability and of this GCM's ability to represent them. If these impacts had been uniform across timescales, then their diagnosis and interpretation would perhaps be relatively simple. However, our subsequent detailed analysis revealed sharply contrasting ENSO impacts on different timescales. This raises the issue of whether different dynamical mechanisms are responsible for these contrasting impacts. We discuss three possibilities below.

On the synoptic scale, changes of variability are usually linked to changes of upper-level jet streams. The ''storm-track'' models of Whitaker and Sardeshmukh (1998) and Branstator (1995) enable a quantitative determination of this link. Specifically, these models predict the changes of synoptic-eddy variance and fluxes given a change in the background flow. As such, they should be ideally suited for assessing the extent to which the patterns of the seasonal-mean response to ENSO (not shown, but discussed in numerous studies, including SCP, and also hinted in Fig. 1) directly determine the patterns of the 500-mb height Δ_σ (synoptic) in Fig. 7. That both the seasonal mean and synoptic variance anomalies are roughly symmetric about the equator is noteworthy in this regard.

Chen and van den Dool (1997a) attributed the greater intraseasonal variability of 500-mb heights in the North Pacific during La Niña to enhanced barotropic energy conversion from the background flow as well as positive synoptic-eddy feedbacks. They pointed to the increases of both synoptic and intraseasonal variance in the Gulf of Alaska as being important in this context (see their Figs. 11 and 12). This is certainly true in the lower panels of our Figs. 6 and 8. However, it is not true in Figs. 7 and 9 in the northern Atlantic or the Southern Hemisphere, where the signs of Δ_σ are opposite for the synoptic and intraseasonal timescales. This suggests that other mechanisms are also at play.

Sardeshmukh et al. (1997), Newman et al. (1997), and Winkler et al. (2001) have demonstrated that barotropic energy conversions alone cannot explain the structure of Northern Hemisphere low-frequency variability, especially the lag-autocovariance structure, without also taking into account the details of the forcing, in particular, tropical diabatic heating. This means that, in addition to altered synoptic-eddy feedbacks, the change of tropical variability in Fig. 9 may also be relevant.

On the seasonal timescale, Chen and van den Dool (1999) hypothesized that an ENSO effect should be similar to that on the intraseasonal (''low frequency'' in their terminology) timescales, ''because the energy spectral shape cannot change much from low-frequency to seasonal timescales.'' This assumption led them to conclude that seasonal predictability in the Pacific North American (PNA) region should increase during El Niño. Renshaw et al. (1998) drew a similar link between changes of intraseasonal and seasonal variability. Our own Fig. 11 and Figs. 4, 5, and 8 strongly indicate that ENSO-induced intraseasonal variance changes *cannot* be used as a proxy for the monthly or seasonal variance changes. Note that Δ_σ (intraseasonal) and Δ_σ (seasonal) are actually of opposite sign in the North Pacific during El Niño (cf. Figs. 9 and 4).

Further analysis toward understanding the changes of variability reported here should account for at least three distinct mechanisms that may be important to varying degrees depending on timescale, region, and details of each ENSO event. Given that tropical forcing in the central equatorial Pacific can generate a large global response, it is at least plausible that ENSO-altered precipitation variability in the region also forces changes in global circulation variability. Changes of tropical rainfall variability alone cannot completely explain our results, however, since the tropical Δ_σ patterns are similar across timescales whereas the extratropical Δ_σ patterns (Figs. 7 and 9) are not. At least two other mechanisms are at work. The mean-state anomalies forced by ENSO affect the structure and location of the Rossby waveguides as well as the dynamical stability of both low- and high-frequency eddies. Also, the altered storm tracks affect the lower-frequency variability through altered synoptic-eddy feedbacks. The relative importance of these three quite different mechanisms can be determined only with further careful diagnosis.

Finally, in addition to understanding the causes of such ENSO-induced changes of variability, it is also important to clarify how they are to be interpreted, especially for individual events. A GCM-generated map of Δ_σ (seasonal) for a particular event, such as Fig. 4, indicates where the ENSO-altered variability enhances or reduces the reliability of an ensemble-mean seasonal forecast. A map of Δ_σ (monthly), as in Fig. 5, may be interpreted similarly. Note that because monthly variances are typically 3 times larger than seasonal variances, Δ_σ (monthly) is typically $\sqrt{3}$ times larger and has a relatively greater impact on the predictability of monthly means. Maps of Δ_σ (intraseasonal) and Δ_σ (synoptic) are better interpreted as the *expected* anomaly of intraseasonal and synoptic variance during a *particular* ENSO season. As such, they should be useful, in conjunction with the mean ENSO signal, for estimating the altered risks of extreme anomalies such as heat waves and cold spells, heavy rains or dry periods, etc., during

that season. The fact that even the relatively low-resolution T40, 18-level GCM used here is sensitive to event-to-event differences of tropical SST forcing encourages further research in this direction.

11. Conclusions

The most important result to emerge from this study is that ENSO-induced changes of atmospheric variability (Δ_σ) are very different across the synoptic to seasonal timescales in the extratropics, but are essentially the same in the Tropics. Regions of statistically significant Δ_σ (synoptic) are more extensive than the rather narrowly defined ''storm tracks'' (e.g., Blackmon et al. 1977) and extend to areas not usually associated with an ENSO effect. The global scale of Δ_σ (intraseasonal) has also not been noticed previously. Some regions, such as the North Atlantic, have Δ_σ of the same sign for El Niño and La Niña. The patterns of Δ_σ (monthly) and Δ_σ (seasonal) are generally similar around the globe, and indicate increased variability during El Niño and decreased variability during La Niña.

We have hypothesized that at least three mechanisms are needed to explain the observed ENSO-induced changes of extratropical variability. First, altered tropical precipitation variability may directly force some of the altered extratropical circulation variability. Second, ENSO-induced changes to the basic state and its stability may alter the dynamics of low-frequency modes such as the PNA and North Atlantic oscillation and also high-frequency eddies. Third, changes to the synoptic-eddy statistics may modify the eddy feedback on low-frequency variability. Most likely, no single mechanism is sufficient. A detailed dynamical diagnosis is needed and is the subject of ongoing research.

Figures 1, 6, and 8 suggest that our case-study GCM approach reasonably represents subseasonal variability and its sensitivity to the phase of ENSO. The separate comparison of El Niño and La Niña with neutral SST conditions has suggested interesting regions where both phases force variability changes of the same sign, such as south Asia, the South Indian Ocean, and the North Atlantic. Differences between the GCM and reanalysis composites may reflect the sensitivity of the atmosphere to details of the anomalous SST forcing, which is blurred by blending disparate ENSO events. Alternatively, the differences may reflect model error. These results will ultimately need to be verified for other ENSO cases and by other GCMs using comparable ensemble sizes.

In closing, we stress again that the predictability of ENSO-induced anomalies on all timescales depends on reliable estimates of both signal *and* noise. Underestimation of the noise will overstate the predictability. Our study (as well as that of SCP) has highlighted the need for large (150 member) ensembles to determine the noise with the necessary accuracy. Finally, the link between the tropical precipitation and extratropical circulation variability hypothesized here suggests that GCM-based seasonal predictions may benefit from improvements in the representation of tropical variability from synoptic to seasonal timescales.

Acknowledgments. The authors are pleased to acknowledge productive conversations with colleagues at CDC, particularly M. Alexander, J. Barsugli, M. Newman, J. Whitaker, and C. Winkler. Assistance with running the NCEP AGCM provided by J. Barsugli and members of NCEP's Coupled Modeling Branch is gratefully acknowledged. R. Livezey of NCEP made useful suggestions for implementing field significance for the present study. The GISST data were kindly provided by D. Rowell and the Hadley Centre of the Met Office. NCEP–NCAR and ECMWF reanalysis data were obtained from the CDC archives (http://www.cdc.noaa.gov) with the assistance of D. Hooper. C. Winkler assisted in the preparation of the chi-corrected data. Three anonymous reviewers made useful comments that improved the present manuscript. This research was partly supported by a grant from NOAA's Office of Global Programs.

APPENDIX

Field Significance Testing

The field significance of the variance changes reported in this paper is assessed using a bootstrap method (resampling with replacement) and the binomial distribution (Livezey and Chen 1983). As suggested by Efron (1982), the mean of the ensemble is removed separately for the El Niño, La Niña, and neutral distributions. For the monthly and seasonal variance changes, 360 ensemble members are pooled (e.g., 180 El Niño and 180 neutral), and two sets of 180 members are randomly drawn. The ratio of variances from the two sets is calculated at every grid point, and the areal coverage is computed from the area-weighted fraction of grid points passing a local F test. The procedure is repeated 2000 times. All monthly and seasonal maps shown are field significant at or above the 10% level (i.e., less than 200 of the 2000 variance-change maps have areal coverage larger than that found for the actual variance change).

For the daily data, to avoid extensive recalculation of thousands of synthetic Fourier transforms, we use the binomial method of Livezey and Chen (1983). We use the field significance of variance ratios of monthly averages described above to estimate the equivalent spatial degrees of freedom (edof) and field significance of synoptic and intraseasonal variance ratios. From the above Monte Carlo for field significance, every month has a distribution of areal coverage of local significant variance ratios. This distribution is compared with a binomial distribution (with parameter $p = 0.1$ corresponding to the 10% local significance level) having some number of edof. Combining January, February, and

March there are a total of six sets of distributions of areal coverage (El Niño and neutral and La Niña and neutral for each month). From inverting the binomial distribution for each of the sample distributions as suggested by Livezey and Chen (1983), we estimate that for variance ratios of 500-mb height monthly averages the edof is between 26 and 62 with a mean value of 42.8. From this we assume that at least 50 edof are appropriate for the 500-mb height bandpass-filtered results. For precipitation, because some regions of monthly, and many regions of daily, precipitation are non-Gaussian, the F test for variance ratios is less appropriate. Still, it does represent a consistent test. The Monte Carlo results suggest between 12 and 18 edof for monthly precipitation variance ratios with an average of 16.0. We assume 18 edof for bandpass-filtered precipitation variance changes. With these assumptions, using the binomial distribution, all bandpass-filtered maps shown are field significant well above the 1% level. At a minimum, assuming 26 edof for 500-mb height and 12 for precipitation, all bandpass-filtered maps are field significant above the 10% level.

REFERENCES

Barnett, T. P., and Coauthors, 1994: Forecasting global ENSO-related climate anomalies. *Tellus,* **46A,** 381–397.

Barsugli, J. J., J. S. Whitaker, A. F. Loughe, P. D. Sardeshmukh, and Z. Toth, 1999: The effect of the 1997/98 El Niño on individual large-scale weather events. *Bull. Amer. Meteor. Soc.,* **80,** 1399–1411.

Blackmon, M. L., J. M. Wallace, N.-C. Lau, and S. L. Mullen, 1977: An observational study of the Northern Hemisphere wintertime circulation. *J. Atmos. Sci.,* **34,** 1040–1053.

Borges, M. D., and P. D. Sardeshmukh, 1995: Barotropic Rossby wave dynamics of zonally varying upper-level flows during northern winter. *J. Atmos. Sci.,* **52,** 3779–3796.

Branstator, G., 1995: Organization of storm track anomalies by recurring low-frequency circulation anomalies. *J. Atmos. Sci.,* **52,** 207–226.

Chen, W. Y., and H. M. van den Dool, 1997a: Asymmetric impact of tropical SST anomalies on atmospheric internal variability over the North Pacific. *J. Atmos. Sci.,* **54,** 725–740.

——, and ——, 1997b: Atmospheric predictability of seasonal, annual, and decadal climate means and the role of the ENSO cycle: A model study. *J. Climate,* **10,** 1235–1254.

——, and ——, 1999: Significant change of extratropical natural variability and potential predictability associated with the El Niño/Southern Oscillation. *Tellus,* **51A,** 790–802.

Dole, R. M., and N. D. Gordon, 1983: Persistent anomalies of the extratropical Northern Hemisphere wintertime circulation: Geographical distribution and regional persistence characteristics. *Mon. Wea. Rev.,* **111,** 1567–1586.

Efron, B., 1982: *The Jackknife, the Bootstrap, and Other Resampling Plans.* SIAM, 92 pp.

Fraedrich, K., 1990: European Grosswetter during the warm and cold extremes of the El Niño/Southern Oscillation. *Int. J. Climatol.,* **10,** 21–31.

——, 1994: An ENSO impact on Europe? A review. *Tellus,* **46A,** 541–552.

Gershunov, A., and T. P. Barnett, 1998: ENSO influence on intraseasonal extreme rainfall and temperature frequencies in the contiguous United States: Observations and model results. *J. Climate,* **11,** 1575–1586.

Gibson, J. K., P. Kąllberg, S. Uppala, A. Hernandez, A. Nomura, and E. Serrano, 1997: ERA description. ECWMF Re-analysis project report series 1, ECMWF Tech. Rep., 872 pp.

Hoerling, M. P., and M. Ting, 1994: Organization of extratropical transients during El Niño. *J. Climate,* **7,** 745–766.

Jenkins, G. M., and D. G. Watts, 1968: *Spectral Analysis and Its Applications.* Holden-Day, 525 pp.

Kalnay, E., and Coauthors, 1996: The NCEP/NCAR 40-Year Reanalysis Project. *Bull. Amer. Meteor. Soc.,* **77,** 437–471.

Kanamitsu, M., and Coauthors, 1991: Description of NMC global data assimilation and forecast system. *Wea. Forecasting,* **6,** 425–435.

Katz, R. W., and B. G. Brown, 1992: Extreme events in a changing climate: Variability is more important than averages. *Climatic Change,* **21,** 289–302.

Kumar, A., M. P. Hoerling, M. Ji, A. Leetma, and P. D. Sardeshmukh, 1996: Asessing a GCM's suitability for making seasonal predictions. *J. Climate,* **9,** 115–129.

Lau, N.-C., 1988: Variability in the observed midlatitude storm tracks in relation to low-frequency changes in the circulation pattern. *J. Atmos. Sci.,* **45,** 2718–2743.

Livezey, R. E., and W. Y. Chen, 1983: Statistical field significance and its determination by Monte Carlo techniques. *Mon. Wea. Rev.,* **111,** 46–50.

Matthews, A. J., and G. N. Kiladis, 1999: Interaction between ENSO, transient circulation, and tropical convection over the Pacific. *J. Climate,* **12,** 3062–3086.

May, W., 1999: Space–time spectra of the atmospheric intraseasonal variability in the extratropics and their dependency on the El Niño Southern Oscillation phenomenon: Model versus observation. *Climate Dyn.,* **15,** 369–387.

——, and L. Bengtsson, 1998: The signature of ENSO in the northern hemisphere midlatitude seasonal mean flow and high-frequency intraseasonal variability. *Meteor. Atmos. Phys.,* **69,** 81–100.

Newman, M., P. D. Sardeshmukh, and C. Penland, 1997: Stochastic forcing of the wintertime extratropical flow. *J. Atmos. Sci.,* **54,** 435–455.

——, ——, and J. W. Bergman, 2000: An assessment of the NCEP, NASA, and ECMWF reanalyses over the tropical western Pacific warm pool. *Bull. Amer. Meteor. Soc.,* **81,** 41–48.

Parker, D. E., C. K. Folland, A. Bevan, M. N. Ward, M. Jackson, and K. Maskell, 1995: Marine surface data for analyses of climate fluctuations on interannual to century time scales. *Natural Climate Variability on Decade to Century Time Scales,* D. G. Martinson et al., Eds., National Academy Press, 241–250.

Renshaw, A. C., D. P. Rowell, and C. K. Folland, 1998: Wintertime low-frequency weather variability in the North Pacific–American sector 1949–93. *J. Climate,* **11,** 1073–1093.

Renwick, J. A., 1998: ENSO-related variability in the frequency of South Pacific blocking. *Mon. Wea. Rev.,* **126,** 3117–3123.

——, and J. M. Wallace, 1996: Relationships between North Pacific wintertime blocking, El Niño, and the PNA pattern. *Mon. Wea. Rev.,* **124,** 2071–2076.

——, and M. J. Revell, 1999: Blocking over the South Pacific and Rossby wave propagation. *Mon. Wea. Rev.,* **127,** 2233–2247.

Reynolds, R. W., and T. M. Smith, 1994: Improved global sea surface temperature analyses using optimum interpolation. *J. Climate,* **7,** 929–948.

Robertson, A. W., and M. Ghil, 1999: Large-scale weather regimes and local climate over the western United States. *J. Climate,* **12,** 1796–1813.

Sardeshmukh, P. D., 1993: The baroclinic chi problem and its application to the diagnosis of atmospheric heating rates. *J. Atmos. Sci.,* **50,** 1099–1112.

——, M. Newman, and M. D. Borges, 1997: Free barotropic Rossby wave dynamics of the wintertime low-frequency flow. *J. Atmos. Sci.,* **54,** 5–23.

——, ——, and C. R. Winkler, 1999: Dynamically consistent estimates of diabatic heating. *Proc. 24th Annual Climate Diagnostics Workshop,* Tucson, AZ, NOAA, 172–175.

——, G. P. Compo, and C. Penland, 2000: Changes of probability associated with El Niño. *J. Climate*, **13,** 4268–4286.
Schubert, S. D., M. J. Suarez, Y. Chang, and G. Branstator, 2001: The impact of ENSO on extratropical low-frequency noise in seasonal forecasts. *J. Climate*, **14,** 2351–2365.
Smith, C. A., and P. D. Sardeshmukh, 2000: The effect of ENSO on the intraseasonal variance of surface temperatures in winter. *Int. J. Climatol.*, **20,** 1543–1557.
Straus, D. M., and J. Shukla, 1997: Variations of midlatitude transient dynamics associated with ENSO. *J. Atmos. Sci.*, **54,** 777–790.
Trenberth, K. E., 1997: The definition of El Niño. *Bull. Amer. Meteor. Soc.*, **78,** 2771–2777.
Vincent, D. G., A. Fink, J. M. Schrage, and P. Speth, 1998: High- and low-frequency intraseasonal variance of OLR on annual and ENSO timescales. *J. Climate*, **11,** 968–986.
Wehner, M. F., 2000: A method to aid in the determination of the sampling size of AGCM ensembles. *Climate Dyn.*, **16,** 321–331.
Whitaker, J. S., and P. D. Sardeshmukh, 1998: A linear theory of extratropical synoptic eddy statistics. *J. Atmos. Sci.*, **55,** 237–258.
Winkler, C. R., M. Newman, and P. D. Sardeshmukh, 2001: A linear model of wintertime low-frequency variability. Part I: Formulation and forecast skill. *J. Climate*, in press.